Ferritin-Based New Magnetic Force Microscopic Probe Detecting 10 nm Sized Magnetic Nanoparticles

Duckhoe Kim,[†,⊥] Nak-Kwan Chung,[†,⊥] Stephanie Allen,[‡] Saul J. B. Tendler,[‡] and Joon Won Park[†,§,*]

[†]Department of Chemistry, Pohang University of Science and Technology, San 31, Hyoja-dong, Pohang, Korea, [‡]Laboratory of Biophysics and Surface Analysis, School of Pharmacy, The University of Nottingham, Nottingham NG7 2RD, United Kingdom, and [§]Division of Integrative Biosciences and Biotechnology, Pohang University of Science and Technology, San 31, Hyoja-dong, Pohang, Korea. [⊥]These authors contributed equally to this work.

ABSTRACT A single-molecule ferritin picking-up process was realized with the use of AFM, which was enhanced by employing controlled dendron surface chemistry. The approach enabled the placement of a single ferritin protein molecule at the very end of an AFM tip. When used for magnetic force microscopy (MFM) imaging, the tips were able to detect magnetic interactions of approximately 10 nm sized magnetic nanoparticles. The single ferritin tip also showed the characteristics of a "multifunctional" MFM probe that can sense the magnetic force from magnetic materials as well as detect the biomolecular interaction force with DNAs on the surface. The multifunctional tip enabled us not only to investigate the specific molecular interaction but also to image the magnetic interaction between the probe and the substrate, in addition to allowing the common capability of topographic imaging. Because the protein engineering of ferritin and the supporting coordination and conjugation chemistry are well-established, we envisage that it would be straightforward to extend this approach to the development of various single magnetic particle MFM probes of different compositions and sizes.

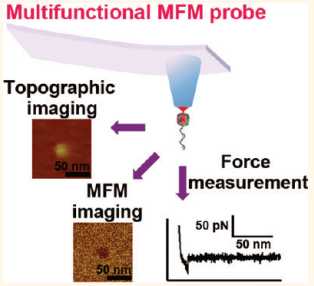

KEYWORDS: single-molecule functionalized AFM probe · single-molecule picking · atomic force microscopy · magnetic force microscopy · multifunctional probe

The ability to interrogate single magnetic nanoparticles (MNPs) has become an increasingly important issue in materials science and biology. In materials science, MNPs have been considered as promising materials for ultrahigh-density recording media and spintronic devices.[1−3] Particularly for magnetic data recording, there has been an intense effort to generate regular 2-D nanoparticle arrays and to develop approaches to detect each individual nanoparticle within the array, wherein a single MNP represents a bit.[4,5] In biological applications, MNPs are commonly used for labeling and sorting target biomolecules.[6−8] Moreover, MNPs conjugated with a ligand have been used for the mapping of receptors on cell surfaces.[9] Nanometer-sized magnetic particles have applications for targeted drug delivery, magnetic resonance imaging of microorganisms, and isolation of labeled targets of interest.[10−12]

Atomic force microscopy (AFM) is a nanomechanical tool that is useful for imaging surfaces at a nanometer level of resolution and for measuring interactions such as the recognition events of a single molecular pair.[13−20] Magnetic force microscopy (MFM) is a derivative of AFM that utilizes the magnetic interaction between the probe and the sample to detect and localize magnetic domains on a substrate, in ambient or buffer conditions.[21,22] The magnetic force-sensing ability of conventional MFM instruments strongly depends on the shape and magnetic property of the MFM probe. In general, commercial MFM probes are coated with magnetic materials such as Co, CoPt, and FePt. The coating layer broadens the tip radius from 5−10 to 20−50 nm and leads to a lower spatial resolution in topography images as compared to those acquired with conventional AFM probes. The relatively strong magnetic moment of commercial MFM probes also distorts the magnetic moment direction of MNPs.[5] Furthermore, MFM detection of MNPs smaller than 20 nm using conventional AFM is beyond current capabilities.[23,24]

One of the most successful approaches reported for enhancing the properties of magnetic tips for MFM used tips functionalized with metal-coated carbon nanotubes (CNTs).[25] The authors demonstrated the sensitivity of such tips to detect line-patterned magnetic domains of 20 nm in width in flat magnetic recording media. However, their ability to image more complex samples and, in particular, to detect spherical MNPs of

* Address correspondence to jwpark@postech.ac.kr.

Received for review September 8, 2011 and accepted December 7, 2011.

Published online December 08, 2011
10.1021/nn203464g

dimensions smaller than 20 nm has not yet been shown. Also, while elegant, this approach is not trivial, requiring the growth and subsequent metallic coating of individual metallic CNTs to AFM tips and an optimization of CNT length to avoid interference from the tip body (which also becomes coated with a magnetic metal coat during this process).[25]

Recently, Garcia and collaborators also demonstrated a bimodal AFM imaging approach that was able to image and detect superparamagnetic nanoparticles.[26] They employed an electronic module which could excite a tip at two different eigenmodes simultaneously. The information from the first eigenmode was used to construct a topographic image, and that from the second was used for investigating the mechanical and magnetic properties of the nanoparticles. Using this approach, the authors could image and detect MNPs down to 5 nm in air or liquid conditions at room temperature. Although the approach required modification to current AFM instrumentation, it demonstrated that AFM can be employed to detect MNPs beyond the previous detection limits if an appropriate method is provided for discriminating between short-range nonmagnetic and long-range magnetic interactions.[27,28] Encouraged by these observations, we focused on fabricating a tip for MFM imaging that could detect MNPs at a distance where nonmagnetic interactions do not interfere. In this report, we present a new approach for manufacturing highly sensitive probes that work in tapping-lift mode as employed in conventional MFM imaging. To achieve this goal, single ferritin molecules were immobilized at the apexes of individual AFM probes. The functionalized probes offered dramatically improved sensitivity for the detection and characterization of MNPs.

RESULTS AND DISCUSSION

Ferritin is an intracellular iron storage protein[29−31] that consists of a 12 nm sized outer shell and an 8 nm sized cavity that can accommodate up to 4500 Fe^{3+} ions. The protein also has been used as a template for the synthesis of various nanoparticles composed of materials such as Co, Ni, Au, Ag, Pt, bimetallic alloys, semiconducting nanocrystals, and metal oxides in aqueous conditions.[32−38] Furthermore, the outer shell can be chemically utilized and conjugated with other materials, such as quantum dots, to form heteronanoconjugates as bifunctional imaging agents.[39] The versatility of ferritin has attracted the interest of researchers as a promising platform for the creation of new nanomaterials.

Recently, AFM was employed not only to pick up single DNA molecules from an inorganic surface[40] but also to pick up and extend single polymer chains and single DNA strands from a virus.[41,42] We have demonstrated that the approach can be applied to place a single-stranded DNA molecule at the apex of an AFM probe through the picking-up process and ligation.[43] Coating the AFM tips with a dendron, which is a structured macromolecule, enhanced the success yield of the process and eliminated the risk of picking up multiple molecules. Also, with the use of the dendron-coating method, the measurement of DNA hybridization events was realized.[44] This approach has been shown to be effective for mapping individual prostate-specific antigens on a surface,[45] titrating a signal-transducing protein with a metabolite to the single-molecule level,[46] mapping mRNAs in a tissue,[47] and revealing the quasi-equilibrium behaviors of a foldamer.[48]

For the attachment of a single ferritin molecule, the approach that was used for the picking up of single DNA molecules was slightly modified (Supporting Information, Figure S1).[43] As the first step, the tip and substrate were treated with *N*-(3-(triethoxysilyl)propyl)-*O*-polyethyleneoxide urethane (TPU) to generate terminal hydroxyl (−OH) groups on the surface. Then, a third-generation dendron (*i.e.*, 27-acid) was introduced on the silylated surface. After introduction of the dendron layer, the protecting group was removed to generate the reactive amine. The dendron-modified tip was biotinylated through a reaction with NHS-$(EG)_4$-biotin. In parallel, the substrate was reacted with amine-modified DNAs (20-mer) by using a cross-linker (*N*,*N*′-disuccinimidyl carbonate). Biotinylated complementary DNAs were hybridized to the DNAs on the substrate, and avidin−ferritin conjugates were produced (Figure 1).

To pick up single avidin−ferritin conjugates, the difference between the unbinding forces of a 20-mer complementary DNA pair (approximately 30 pN)[44] and the avidin−biotin interaction (>160 pN)[49,50] was exploited (Figure 1a). Biotinylated probes approached the substrate, such that the biotin at the AFM tip apex interacted with an avidin moiety conjugated to a ferritin on the substrate surface. Retraction of the probe from the surface resulted in dehybridization of the 20-mer DNA pair in preference to the avidin−biotin bond, due to the smaller unbinding force, resulting in the transport of a single avidin−ferritin conjugate to the tip.

Because the formation and rupture of biomolecular bonds is a stochastic process, it cannot be guaranteed that "pick-up" will occur on every probe−sample contact cycle. Therefore, to ensure that a ferritin molecule was picked up, the cycle (approach and retract) was repeated at different positions until the single specific unbinding force was observed (Figure 1e). When the specific force was observed, the tip was removed from the AFM and inspected for the presence of a ferritin molecule by utilizing transmittance electron microscopy (TEM). As shown in Figure 1d, the ferritin molecules were imaged as a dark spots, due to their iron cores. Twenty out of the 25 tips functionalized using this approach showed a single ferritin molecule, and no multiple ferritins were observed (success yield: 75%).

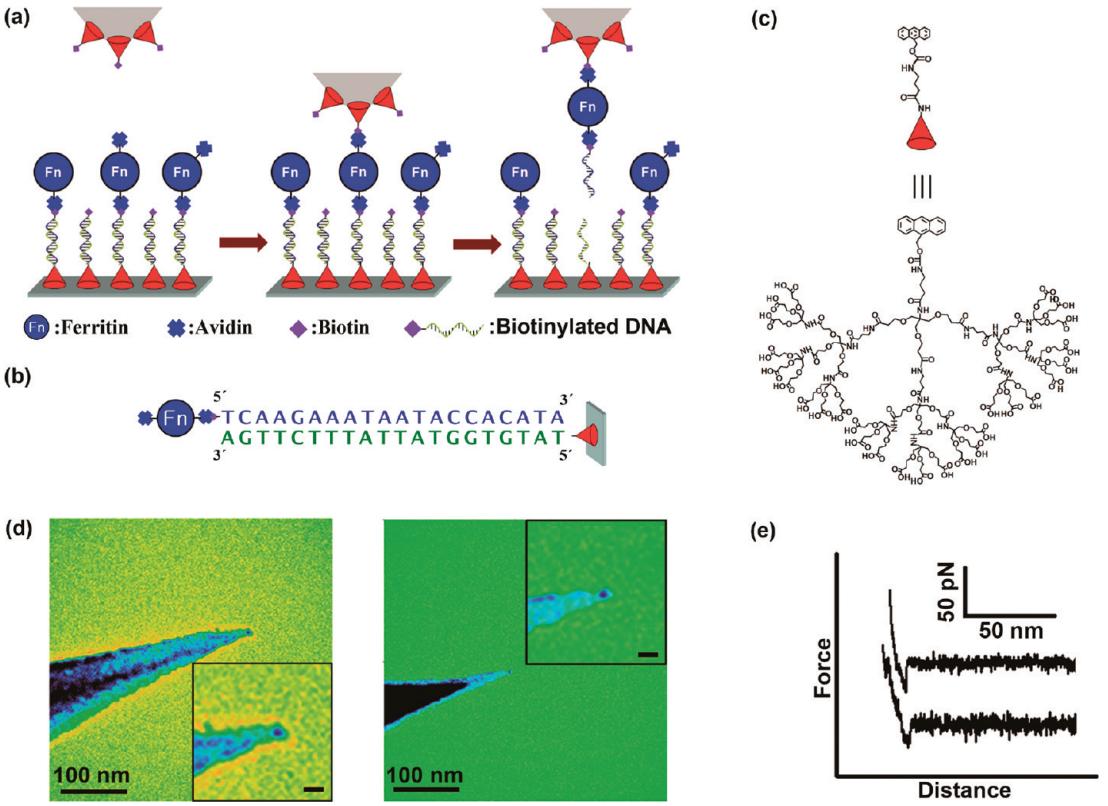

Figure 1. Picking up an avidin–ferritin conjugate. (a) Schematic diagram for the picking-up process. (b) DNA sequences used for the ferritin immobilization on a substrate. (c) Structure of the dendron molecule used for the tip and substrate modifications. (d) TEM images of AFM tips after ferritin attachment. A dark spot at the apex of a tip is evident (inset scale bar: 10 nm). (e) Specific force curves, corresponding to the rupture of the hybridized DNA complex, were observed during the picking-up process.

In general, the quantity of Fe^{3+} ions in the core varies among ferritin molecules, and some ferritins even have an empty core. When using this approach, there is always a risk of picking up an avidin–ferritin conjugate with no iron core; this is one of the reasons that the yield is not 100% (Supporting Information, Figure S2). It is also worth noting that ferritin molecules were always found at the apex of the tip. We attribute this fact to the use of a shorter linker NHS-(EG_4-biotin) than was used in previous DNA picking-up experiments.

For the MFM imaging, we employed the tapping-lift mode, initially with AFM probes derivatized with native ferritin molecules. In the tapping-lift mode, the parameters are first optimized in tapping mode so as to obtain the highest quality topography images. The oscillating tip is first traced and retraced along a scan line to obtain topographic information. To obtain the magnetic image data, the tip is then raised to a chosen lift height above the sample and scanned again along the same line but maintaining the tip–sample separation at the chosen value throughout the second scan. This process should remove any signal arising from variation in sample topography from the second trace, allowing any variation in cantilever oscillation (*e.g.*, amplitude or phase) to be attributed to changes in the magnetic force between the tip and the surface.

The AFM probes that were optimal for the ferritin picking-up process and for observing the specific DNA–DNA interaction forces were conventional "contact mode" AFM cantilevers. Unfortunately, when used for tapping mode imaging in an ambient environment, such probes frequently failed the autotune control instrumental process that searches the cantilever excitation spectrum for the location of appropriate resonance frequency peaks to enable tapping mode imaging, and all parameters had to be tuned manually. In the case of manual calibration, the exact control of the drive phase, which is needed to set the parameters required for the acquisition of phase images, was difficult. For these reasons, the amplitude signal was mainly employed for the MFM imaging. However, the phase signal for the MFM imaging was also attainable with probes that were compatible with the autotune control process.

A test sample was prepared by the physisorption of magnetic (Fe_3O_4) nanoparticles, 5–15 nm in diameter, on a silicon substrate. While TEM analysis confirmed the size, topographic AFM imaging showed particles of 20–30 nm in height on a substrate. It was evident that some particles aggregated during the physisorption. For MFM imaging, native ferritin-functionalized tips and MNPs needed to be magnetized with a permanent

magnet. In general, MNPs of less than 30 nm are superparamagnetic and can maintain their magnetization only in the presence of an external magnetic field at room temperature. In the case of the employed microscope, a built-in magnet in the sample holder generated a magnetic field directed perpendicular to the substrate, which was sufficient to maintain the magnetization of the particles.[24] As a result, the native ferritin tip could detect an MNP at a 50 nm lift height, which, from the topography image, had a height of 21.1 nm. When the magnetic field from the holder was shielded with a metal plate as a control, the same tip could not detect any MNPs above the lift height of 20 nm (Supporting Information, Figure S3). These data confirmed that the external magnetic field was a prerequisite to detect MNPs for the MFM imaging[24] and also indicate that signals in the lift mode originated only from the magnetic interaction.

Further experiments were performed to investigate the impact of reducing the ferritin core. According to a previous report, thermal reduction of the Fe^{3+} precursor generates a ferromagnetic mixture of Fe_3C and Fe phases.[51] In the case of reduction of the core of ferritin molecules (a mixture of ferrihydrite, hematite, and magnetite), formation of the same phases has also been reported.[52] To confirm this process within these studies, ferritin powder was placed in a chemical vapor deposition chamber, annealed to 800 °C, and incubated for 5 min with H_2 flow. The X-ray diffraction (XRD) pattern of the resulting powder indicated the formation of a mixture of iron species, identical to that previously reported. These reduction conditions were then applied to tips functionalized with native ferritin molecules (Supporting Information, Figure S4), and the resultant reduced tips were employed for the MFM imaging of MNPs. With the reduced iron tip, a MNP of 9.4 nm could be detected at a lift height of 50 nm (Figure 2). The ability to detect MNPs as small as 9.4 nm is a significant improvement over that achievable using the currently available MFM probes. The theoretical detection limit of conventional MFM[23,24] is around 15 nm; however, in practice, only MNPs and aggregates of a much larger size can be detected.[24]

To confirm that the detection of MNPs with the reduced iron tip did not originate from nonmagnetic interactions, images of nonmagnetized and magnetized MNPs were obtained with the same tip (Supporting Information, Figure S5). For the imaging of nonmagnetized MNPs, the magnetization process was skipped and the external field from the sample holder was shielded with a metal plate. In this case, the reduced iron tip could not detect the nonmagnetized MNP at a lift height of 50 nm. However, when the probe and sample were magnetized, the same tip could detect MNPs as small as 11.6 nm at the same lift height. We also examined nonmagnetic SiO_2 nanoparticles for MFM imaging with the reduced iron tip. The result was

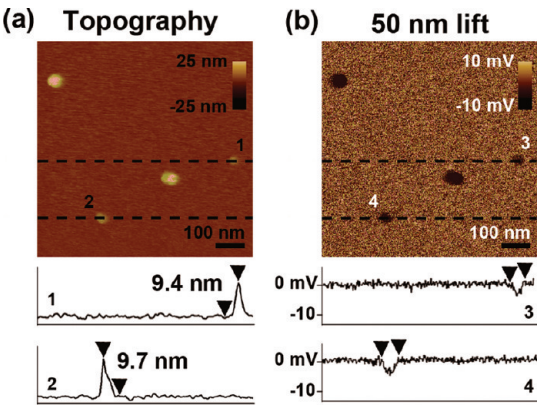

Figure 2. (a) Topographic and (b) corresponding MFM image of magnetic nanoparticles scanned with a reduced iron tip. The vertical height of features was measured to estimate the particle size. Below each topographic and MFM image, line profiles along the dashed lines are displayed.

identical to the case of nonmagnetized MNPs. These results strongly support the hypothesis that the detection of MNPs in the lift mode was due to the magnetic interaction between the tip and the MNP.

Furthermore, it was found that the presence of only a single magnetic particle on the AFM tip was critical for the improvement of the sensitivity. As a further control, a biotinylated tip was completely immersed in an avidin–ferritin solution to generate a tip functionalized with multiple ferritin molecules (Supporting Information, Figure S6). After reduction, the tip with multiple particles was used for the detection of MNPs and showed a poor sensitivity. The control experiment clarified that the improved sensitivity originated from the single magnetic particle on the tip. One possible interpretation is that the magnetic field from a single domain can be stretched out further, whereas this is not the case for the field from multiple domains. Magnetic fields from multiple domains can interact with each other, resulting in a loop formation of the magnetic field lines near the tip surface. This situation might reduce the magnetic interactions between the tip and the MNP on the substrate when the tip is raised and scanned in the lift mode.

However, it should be noted that careful choice was required to obtain good quality images of sample topography when using the ferritin/reduced ferritin functionalized probes. We employed probes with spring constants from 0.01 to 0.03 N/m to enable the required observation of specific DNA–DNA unbinding events. These probes had resonance frequencies of 9–15 kHz. In general, tapping mode topographic imaging with such soft probes was not stable because the imaging tip could easily adhere to the substrate due to the presence of the surface water (or capillary) layer which exists on surfaces in ambient environments. Moreover, we employed light tapping conditions; typically a 70–80% reduction in cantilever oscillation amplitude was used as the set point. Under these conditions, dryness of a

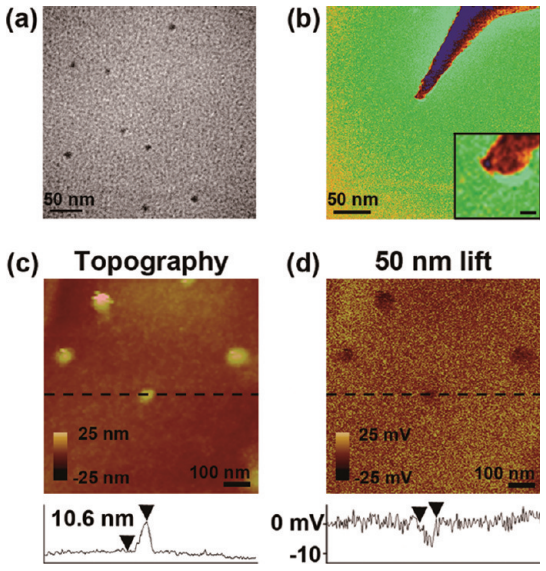

Figure 3. (a) TEM image of apoferritin molecules containing synthesized Co(0) nanoparticles. (b) TEM image of the Co(0)–ferritin-functionalized AFM tip. A dark spot at the apex (upper surface, left-hand side) of the tip is discernible (inset scale bar: 10 nm). (c) Topographic image and (d) corresponding MFM images of magnetic nanoparticles obtained with a Co(0)–ferritin tip. Below each topographic and MFM image, a line profile corresponding to the dashed line is displayed.

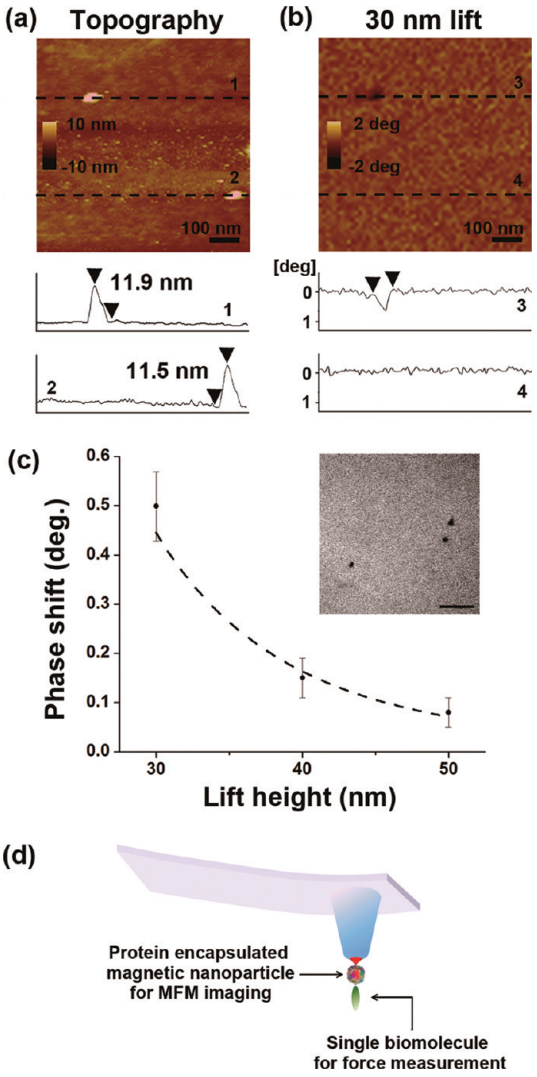

Figure 4. (a) Topographic image and (b) corresponding MFM image of a mixture of AuNP and magnetic nanoparticles obtained with a Co(0)–ferritin tip. Below the images, line profiles along the dashed lines in each image are displayed. (c) Plot of the phase shift as a function of lift height. The dashed line is the fit of the phase shift value to eq 1 using Q = 70 and k = 0.020 N m^{-1}. The inset image shows a TEM image of the distribution of magnetic nanoparticles on surface (inset scale bar: 50 nm). (d) Schematic diagram of the proposed "multifunctional" probe.

substrate and a low humidity were essential to obtain the topographic images. In addition, selection of a probe with a higher resonance frequency enhanced the success rate. In the case of probes that had resonance frequencies of less than 10 kHz, only 20–30% of the probes could successfully obtain a topographic image. Probes with resonance frequencies larger than 10 kHz were more successful, and probes with frequencies larger than 12 kHz always gave topographic images. Therefore, if both magnetic and topography images were required, the selection of probes of a higher frequency was needed.

As an extension of this approach, we created a cobalt (0) nanoparticle within the apoferritin structure[32] and followed the above procedure for tip functionalization. Cobalt is the most commonly used material for coating commercially available MFM probes. For our approach, if a tip having a Co nanoparticle encapsulated by apoferritin performed as well as the reduced ferritin tip, then it would be possible to skip the thermal reduction procedure, while retaining the protein shell that could be utilized for other applications.[39] After its preparation, Co(0)–ferritin was reacted with NHS-$(EG)_{12}$-biotin to enable further conjugation with avidin.

The TEM results showed the uniformity of the core of the Co(0)-containing ferritin–avidin conjugates (Figure 3a). As shown in the figure, the conjugates were completely isolated from each other, without forming agglomerates that would be expected to occur if cobalt ions were not encapsulated by the apoferritin shell. Prepared Co(0)–ferritin–avidin conjugates were used for the picking-up process, and the presence of a single Co(0)–ferritin was confirmed by TEM (Figure 3b). As with the experiments with native ferritin, single Co nanoparticles were also observed at the very end of the tips, and a similar picking-up yield was observed (eight out of 11 tips). In the MFM imaging with the Co(0)–ferritin tip, the tip showed comparable performance and could detect MNPs as small as 10.6 nm.

The magnetic moment of the detected MNPs can be estimated from the MFM imaging with the Co(0)–ferritin tip. The relationship between the MFM signal and the lift height[24] can be expressed as

$$\delta\varphi = \frac{\mu_0}{4\pi}\frac{12\pi Q}{k(h+c)^5} m_p m_s \frac{180}{\pi} \qquad (1)$$

where k is the spring constant of the MFM cantilever and Q is its quality factor; μ_0 is the permeability of a vacuum; h is the lift height; c is a constant related to the ferritin shell thickness, the radius of the MNP, and the ferritin core; m_s is the magnetic moment of a magnetic nanoparticle; and m_p is the probe magnetic moment, given as

$$m_p = \frac{4}{3}\pi R^3 M_p \quad (2)$$

where M_p (1.4×10^6 A m^{-1}) is the saturation magnetization of Co, and R (*ca.* 3.0 nm) is the radius of the Co core in a ferritin. Using eq 2, m_p was estimated to be approximately 1.6×10^{-19} A m^2.

To use eq 1, the phase shift (rather than the amplitude) needs to be measured during lift mode imaging. To achieve this goal, we selected a Co(0)–ferritin tip that was compatible with the autotune control process of the instrument (Supporting Information, Figure S7). It was also important to know the lowest lift height at which only magnetic interactions could be detected (*e.g.*, so that the influence of other tip–sample interactions on the observed contrast could be excluded). To clarify the lift height, we imaged a surface on which 10 nm gold and magnetite nanoparticles had been deposited using the Co(0)–ferritin tip (Figure 4). As shown, only the latter particle induced a phase shift at a lift height of 30 nm. This result is unambiguous evidence that nonmagnetic probe–sample interactions could be completely excluded beyond a lift height of 30 nm (Supporting Information, Figure S8). It also indicates that the lateral resolution of the MFM imaging with the Co(0)–ferritin tip is about 30 nm in this particular circumstance. In general, the level of lateral resolution achievable in MFM imaging decreases by a factor comparable to the lift height when lift mode is used. Because the Co(0)–ferritin tip could sense the magnetic interaction only above the lift height of 30 nm, each 10 nm MNP therefore needed to be separated from the others by a distance of at least 30 nm to avoid nonmagnetic interference.

Figure 4c presents the phase shift of the same Co(0)–ferritin tip induced by MNPs as a function of the lift height from 30 to 50 nm, in 10 nm increments. The average height of the MNPs in the experiment was 12.1 ± 1.3 nm. The dashed line in Figure 4c shows the fitted curve predicted by eq 1. From the fitting, the calculated average magnetic moment was 6.9×10^{-19} A m^2, which is close to the extrapolated value (4.4×10^{-19} A m^2) from the literature.[24,53] The good agreement between these values supports the hypothesis that the phase shift originated from the magnetic interaction alone.

In parallel with these experiments, we also investigated the distribution of MNPs on a surface with TEM. As shown in the inset image of Figure 4c, MNPs existed as isolated features on the physisorbed surface. These observations clearly demonstrate that the AFM probe tips functionalized with Co(0)–ferritin could detect a single MNP. Moreover, the Co(0)–ferritin tip and the native ferritin tip were initially used for the recognition of specific DNA–DNA interactions in buffer conditions and then used for the detection of MNPs in the ambient condition without any further treatment.[54] This result indicates that the Co(0)–ferritin tip and the native ferritin tip are already good examples of a multifunctional probe (Figure 4d) that can sense magnetic force from magnetic materials and can detect the biomolecular interaction force with DNAs on the surface. A multifunctional tip enables us not only to investigate the specific molecular interaction but also to image the magnetic interaction between the probe and the substrate, in addition to its common capability of topographic imaging.

In summary, we have demonstrated a new approach to place a single ferritin molecule with a magnetic core on AFM tips, through the use of the underlying dendron surface functionality. This approach enhanced the reliability and reproducibility of the molecular pick-up process. The approach also enabled the placement of single proteins only at the apex of the AFM tips, providing a new type of MFM probe capable of detecting 10 nm sized MNPs. Because the protein engineering of ferritin and the supporting coordination and conjugation chemistry are well-established, we envisage that it would be straightforward to extend this approach to the development of various single magnetic particle MFM probes of different compositions and sizes.

METHODS

General. The silane coupling agent *N*-(3-(triethoxysilyl)-propyl)-*O*-polyethyleneoxide urethane (TPU) was purchased from Gelest. Magnetic nanoparticle colloids were purchased from ChemiCell. NHS-$(EG)_n$-biotin linker was purchased from Thermo Scientific. Avidin (from egg white) conjugated to equine spleen ferritin (lyophilized powder) and apoferritin colloids (from equine spleen) were purchased from Sigma-Aldrich. For the preconjugated material, approximately 1.0 mol of ferritin molecule was labeled with 1.6 mol of avidin (as stated by the manufacturer). All other chemicals were of reagent grade from Sigma-Aldrich. Oligonucleotides were purchased from Bionics. The AFM probes employed for the picking-up process were purchased from Applied NanoStructures, Nanosensors, and Bruker Nano. MSNC-MF probe (Bruker Nano) and SSS-MFMR probe (Nanosensors) were used for MFM imaging. Transmission electron microscopy (JEM-1011, JEOL) was used to image AFM tips.

Sample Preparation. Dendron-modified probes and substrates were prepared as reported previously.[40] For the preparation of biotinylated tips, the dendron-modified AFM probes were reacted with 3.4 mM NHS-$(EG)_4$-biotin in PBST buffer (10 mM phosphate buffer, 2.7 mM KCl, 137 mM NaCl, 0.05% Tween 20, pH 8.5) containing 2 mM ethylenediaminetetraacetate for 4 h. The biotinylated cantilevers were rinsed with PBST buffer

and deionized water. Finally, the cantilevers were dried under vacuum (30−40 mTorr). For the preparation of ferritin-immobilized substrate, a substrate functionalized with a probe DNA was prepared as reported previously.[40] The substrate was hybridized with a complementary biotinylated DNA (20 nM in a hybridization buffer [2× SSPE buffer containing 7.0 mM sodium dodecylsulfate, pH 7.4]) at 45 °C for 1 h. Substrates were washed with 20 mL of the hybridization buffer and shaken gently in 2× SSPE buffer solution at 45 °C for 1 min to remove nonspecifically bound oligonucleotides. The sequences of oligonucleotides used for the substrate preparation are presented in Figure 1b. After washing, the substrates were placed in the avidin−ferritin conjugate solution (0.1 mg in 1 mL of $NaHCO_3$ solution [25 mM, pH 8.5] containing 5 mM $MgCl_2$) for 10 min to generate ferritin-functionalized substrates. The resulting substrates were washed with $NaHCO_3$ solution (25 mM, pH 8.5) containing 5 mM $MgCl_2$ and shaken gently in the same $NaHCO_3$ solution at 45 °C for 1 min to remove nonspecifically bound avidin−ferritin conjugates. Substrates were stored in $NaHCO_3$ solution (25 mM, pH 8.5) containing 5 mM $MgCl_2$ prior to their use.

Synthesis of Co(0)-Containing Avidin−Ferritin Conjugate. For the synthesis of the Co(0)-containing ferritins, the previously reported method was adopted.[31] For conjugation of the Co(0)−ferritin with avidin, the Co(0)−ferritin solution was dialyzed in PBS buffer (pH 7.4), and 5 mg of the NHS-$(EG)_{12}$-biotin linker was added to the solution. After 4 h, the solution was dialyzed in $NaHCO_3$ buffer (pH 8.5) containing 5 mg of $MgCl_2$, and a 3500 MWCO Slide-A-Lyzer cassette (ThermoFischer) was used to remove the unreacted linker material. Finally, 10 mg of avidin was dissolved in the dialyzed solution. After 1 h, unreacted avidin was removed by filtration with a 100 000 MWCO Vivaspin. The resulting avidin−ferritin conjugates were concentrated by an identical filtration process.

AFM Experiments for the Picking Up of Single Ferritin Molecules. Ferritin picking was performed with a NanoWizard AFM (JPK Instruments) in $NaHCO_3$ buffer (25 mM, pH 8.5) containing 5 mM $MgCl_2$ at room temperature. To enable the pick-up of ferritin molecules, force measurements were recorded between biotinylated AFM probes and substrates functionalized with avidin−ferritin conjugates. The tip velocity was fixed at 0.20 μm/s, and the z-range was set to 500 nm.

MFM Experiments. The MFM measurements were performed in a tapping-lift mode on a Nanoscope IIIa MultiMode scanning probe microscope (Bruker Nano Corp.). The cantilever oscillation amplitude was 50−60 nm. Surface topography was mapped in the tapping mode during the first pass, and the corresponding MFM signals were acquired on the second pass. For the latter, a tip was lifted by a given distance from the average height of the topographic line profile. To minimize the influence of humidity, every MFM experiment was performed in a chamber in which the humidity was ensured to be lower than 10% by placing anhydrous $CaSO_4$ powder in the chamber.

Acknowledgment. This research was supported by the World Class University (WCU) program through the National Research Foundation of Korea funded by the Ministry of Education, Science, and Technology (R31-2008-000-10105), BK21, and NRF/MEST (2011-0002186).

Supporting Information Available: Additional information about surface preparation, TEM images of AFM tips and MNPs, MFM images with the ferritin tips, and a force histogram is provided. This material is available free of charge *via* the Internet at http://pubs.acs.org.

REFERENCES AND NOTES

1. Sun, S.; Murray, C. B. Synthesis of Monodisperse Cobalt Nanocrystals and Their Assembly into Magnetic Superlattices. *J. Appl. Phys.* **1999**, *85*, 4325–4330.
2. Sun, S.; Murray, C. B.; Weller, D.; Folks, L.; Moser, A. Monodisperse FePt Nanoparticles and Ferromagnetic FePt Nanocrystal Superlattices. *Science* **2000**, *287*, 1989–1992.
3. Kiselev, S. I.; Sankey, J. C.; Krivorotov, I. N.; Emley, N. C.; Schoelkopf, R. J.; Buhrman, R. A.; Ralph, D. C. Microwave Oscillations of a Nanomagnet Driven by a Spin-Polarized Current. *Nature* **2003**, *425*, 380–383.
4. Puntes, V. F.; Krishnan, K. M.; Alivisatos, A. P. Synthesis, Self-Assembly, and Magnetic Behavior of a Two-Dimensional Superlattice of Single-Crystal ε-Co Nanoparticles. *Appl. Phys. Lett.* **2001**, *78*, 2187–2189.
5. Puntes, V. F.; Gorostiza, P.; Aruguete, D. M.; Bastus, N. G.; Alivisatos, A. P. Collective Behaviour in Two-Dimensional Cobalt Nanoparticle Assemblies Observed by Magnetic Force Microscopy. *Nat. Mater.* **2004**, *3*, 263–268.
6. Song, E. Q.; Hu, J.; Wen, C. Y.; Tian, Z. Q.; Yu, X.; Zhang, Z. L.; Shi, Y. B.; Pang, D. W. Fluorescent-Magnetic-Biotargeting Multifunctional Nanobioprobes for Detecting and Isolating Multiple Types of Tumor Cells. *ACS Nano* **2011**, *5*, 761–770.
7. Wittrup, A.; Zhang, S. H.; Svensson, K. J.; Kucharzewska, P.; Johansson, M. C.; Morgelin, M.; Belting, M. Magnetic Nanoparticle-Based Isolation of Endocytic Vesicles Reveals a Role of the Heat Shock Protein GRP75 in Macromolecular Delivery. *Proc. Natl. Acad. Sci. U.S.A.* **2010**, *107*, 13342–13347.
8. Martinez-Morales, A. A.; Portney, N. G.; Zhang, Y.; Destito, G.; Budak, G.; Ozbay, E.; Manchester, M.; Ozkan, C. S.; Ozkan, M. Synthesis and Characterization of Iron Oxide Derivatized Mutant Cowpea Mosaic Virus Hybrid Nanoparticles. *Adv. Mater.* **2008**, *20*, 4816–4820.
9. Moskalenko, A. V.; Yarova, P. L.; Gordeev, S. N.; Smirnov, S. V. Single Protein Molecule Mapping with Magnetic Atomic Force Microscopy. *Biophys. J.* **2010**, *98*, 478–487.
10. Liong, M.; Lu, J.; Kovochich, M.; Xia, T.; Ruehm, S. G.; Nel, A. E.; Tamanoi, F.; Zink, J. I. Multifunctional Inorganic Nanoparticles for Imaging, Targeting, and Drug Delivery. *ACS Nano* **2008**, *2*, 889–896.
11. Wang, Y.; Ng, Y. W.; Chen, Y.; Shuter, B.; Yi, J.; Ding, J.; Wang, S.; Feng, S. S. Formulation of Superparamagnetic Iron Oxides by Nanoparticles of Biodegradable Polymers for Magnetic Resonance Imaging. *Adv. Funct. Mater.* **2008**, *18*, 308–318.
12. Hill, H. D.; Vega, R. A.; Mirkin, C. A. Nonenzymatic Detection of Bacterial Genomic DNA Using the Bio Bar Code Assay. *Anal. Chem.* **2007**, *79*, 9218–9223.
13. Sedman, V. L.; Adler-Abramovich, L.; Allen, S.; Gazit, E.; Tendler, S. J. B. Direct Observation of the Release of Phenylalanine from Diphenylalanine Nanotubes. *J. Am. Chem. Soc.* **2006**, *128*, 6903–6908.
14. Blunt, M. O.; Martin, C. P.; Ahola-Tuomi, M.; Pauliac-Vaujour, E.; Sharp, P.; Nativo, P.; Brust, M.; Moriarty, P. J. Coerced Mechanical Coarsening of Nanoparticle Assemblies. *Nat. Nanotechnol.* **2007**, *2*, 167–170.
15. Hill, R. J. A.; Sedman, V. L.; Allen, S.; Williams, P. M.; Paoli, M.; Adler-Abramovich, L.; Gazit, E.; Eaves, L.; Tendler, S. J. B. Alignment of Aromatic Peptide Tubes in Strong Magnetic Fields. *Adv. Mater.* **2007**, *19*, 4474–4479.
16. Sahin, O.; Magonov, S.; Su, C.; Quate, C. F.; Solgaard, O. An Atomic Force Microscope Tip Designed To Measure Time-Varying Nanomechanical Forces. *Nat. Nanotechnol.* **2007**, *2*, 507–514.
17. Husale, S.; Persson, H. H. J.; Sahin, O. DNA Nanomechanics Allows Direct Digital Detection of Complementary DNA and microRNA Targets. *Nature* **2009**, *462*, 1075.
18. Hinterdorfer, P.; Dufrêne, Y. F. Detection and Localization of Single Molecular Recognition Events Using Atomic Force Microscopy. *Nat. Methods* **2006**, *3*, 347–355.
19. Struckmeier, J.; Wahl, R.; Leuschner, M.; Nunew, J.; Janovjak, H.; Geisler, U.; Hofmann, G.; Jähnke, T.; Müller, D. J. Fully Automated Single-Molecule Force Spectroscopy for Screening Applications. *Nanotechnology* **2008**, *19*, 384020.
20. Müller, D. J.; Dufrêne, Y. F. Force Nanoscopy of Living Cells. *Curr. Biol.* **2011**, *21*, R212–R216.
21. Martin, Y.; Wickramasinghe, H. K. Magnetic Imaging by ``Force Microscopy'' with 1000 Å Resolution. *Appl. Phys. Lett.* **1987**, *50*, 1455–1457.
22. Giles, R.; Cleveland, J. P.; Manne, S.; Hansma, P. K.; Drake, B.; Maivald, P.; Boles, C.; Gurley, J.; Elings, V. Noncontact Force Microscopy in Liquids. *Appl. Phys. Lett.* **1993**, *63*, 617–618.

23. Rasa, M.; Kuipers, B. W. M.; Philipse, A. P. Atomic Force Microscopy and Magnetic Force Microscopy Study of Model Colloids. *J. Colloid Interface Sci.* **2002**, *250*, 303–315.
24. Schreiber, S.; Savla, M.; Pelekhov, D. V.; Iscru, D. F.; Selcu, C.; Hammel, P. C.; Agarwal, G. Magnetic Force Microscopy of Superparamagnetic Nanoparticles. *Small* **2008**, *4*, 270–278.
25. Deng, Z.; Yenilmez, E.; Leu, J.; Hoffman, J. E.; Straver, E. W. J.; Dai, H.; Moler, K. A. Metal-Coated Carbon Nanotube Tips for Magnetic Force Microscopy. *Appl. Phys. Lett.* **2004**, *85*, 6263.
26. Dietz, C.; Herruzo, E. T.; Lozano, J. R.; Garcia, R. Nanomechanical Coupling Enables Detection and Imaging of 5 nm Superparamagnetic Particle in Liquid. *Nanotechnology* **2011**, *22*, 125708.
27. Li, J. W.; Cleveland, J. P.; Proksch, R. Bimodal Magnetic Force Microscopy: Separation of Short and Long Range Forces. *Appl. Phys. Lett.* **2009**, *94*, 163118.
28. Neves, C. S.; Quaresma, P.; Baptista, P. V.; Carvalho, P. A.; Araújo, J. P.; Pereira, E.; Eaton, P. New Insights into the Use of Magnetic Force Microscopy To Discriminate between Magnetic and Nonmagnetic Nanoparticles. *Nanotechnology* **2010**, *21*, 305706.
29. Chasteen, N. D.; Harrison, P. M. J. Mineralization in Ferritin: An Efficient Means of Iron Storage. *J. Struct. Biol.* **1999**, *126*, 182–194.
30. Liu, X.; Theil, E. C. Ferritins: Dynamic Management of Biological Iron and Oxygen Chemistry. *Acc. Chem. Res.* **2005**, *38*, 167–175.
31. Gálvez, N.; Fernández, B.; Sánchez, P.; Cuesta, R.; Ceolín, M.; Clemente-León, M.; Trasobares, S.; López-Haro, M.; Calvino, J. J.; Stéphan, O.; *et al.* Comparative Structural and Chemical Studies of Ferritin Cores with Gradual Removal of Their Iron Contents. *J. Am. Chem. Soc.* **2008**, *130*, 8062–8068.
32. Gálvez, N.; Sánchez, P.; Domínguez-Vera, J. M.; Soriano-Portillo, A.; Clemente-León, M.; Coronado, E. Apoferritin-Encapsulated Ni and Co Superparamagnetic Nanoparticles. *J. Mater. Chem.* **2006**, *16*, 2757–2761.
33. Shin, Y.; Dohnalkova, A.; Lin, Y. Preparation of Homogeneous Gold−Silver Alloy Nanoparticles Using the Apoferritin Cavity as a Nanoreactor. *J. Phys. Chem. C* **2010**, *114*, 5985–5989.
34. Zhang, L.; Laug, L.; Münchgesang, W.; Pippel, E.; Gösele, U.; Brandsch, M.; Knez, M. Reducing Stress on Cells with Apoferritin-Encapsulated Platinum Nanoparticles. *Nano Lett.* **2010**, *10*, 219–223.
35. Gálvez, N.; Valero, E.; Ceolin, M.; Trasobares, S.; López-Haro, M.; Calvino, J. J.; Domínguez-Vera, J. M. A Bioinspired Approach to the Synthesis of Bimetallic CoNi Nanoparticles. *Inorg. Chem.* **2010**, *49*, 1705–1711.
36. Douglas, T.; Stark, V. T. Nanophase Cobalt Oxyhydroxide Mineral Synthesized within the Protein Cage of Ferritin. *Inorg. Chem.* **2000**, *39*, 1828–1830.
37. Kim, J. W.; Choi, S. H.; Lillehei, P. T.; Chu, S. H.; King, G. C.; Watt, G. D. Cobalt Oxide Hollow Nanoparticles Derived by Bio-Templating. *Chem. Commun.* **2005**, 4101–4103.
38. Hennequin, B.; Turyanska, L.; Ben, T.; Beltrán, A. M.; Molina, S. I.; Li, M.; Mann, S.; Patanè, A.; Thomas, N. R. Aqueous Near-Infrared Fluorescent Composites Based on Apoferritin-Encapsulated PbS Quantum Dots. *Adv. Mater.* **2008**, *20*, 3592–3596.
39. Fernández, B.; Gálvez, N.; Cuesta, R.; Hungría, A. B.; Calvino, J. J.; Domínguez-Vera, J. M. Quantum Dots Decorated with Magnetic Bionanoparticles. *Adv. Funct. Mater.* **2008**, *18*, 3931–3935.
40. Kufer, S. K.; Puchner, E. M.; Gumpp, H.; Liedl, T.; Gaub, H. E. Single-Molecule Cut-and-Paste Surface Assembly. *Science* **2008**, *319*, 594–596.
41. Liu, N.; Peng, B.; Lin, Y.; Su, Z.; Niu, Z.; Wang, Q.; Zhang, W.; Li, H.; Shen, J. Pulling Genetic RNA out of Tobacco Mosaic Virus Using Single-Molecule Force Spectroscopy. *J. Am. Chem. Soc.* **2010**, *132*, 11036–11038.
42. Liu, K.; Song, Y.; Feng, W.; Liu, N.; Zhang, W.; Zhang, X. Extracting a Single Polyethylene Oxide Chain from a Single Crystal by a Combination of Atomic Force Microscopy Imaging and Single-Molecule Force Spectroscopy: Toward the Investigation of Molecular Interactions in Their Condensed States. *J. Am. Chem. Soc.* **2011**, *133*, 3226–3229.
43. Kim, D.; Chung, N. K.; Kim, J. S.; Park, J. W. Immobilizing a Single DNA Molecule at the Apex of AFM Tips through Picking and Ligation. *Soft Matter* **2010**, *6*, 3979–3984.
44. Jung, Y. J.; Hong, B. J.; Zhang, W.; Tendler, S. J. B.; Williams, P. M.; Allen, S.; Park, J. W. Dendron Arrays for the Force-Based Detection of DNA Hybridization Events. *J. Am. Chem. Soc.* **2007**, *129*, 9349–9355.
45. Roy, D.; Kwon, S. H.; Kwak, J. W.; Park, J. W. "Seeing and Counting" Individual Antigens Captured on a Micro-arrayed Spot with Force-Based Atomic Force Microscopy. *Anal. Chem.* **2010**, *82*, 5189–5194.
46. Kim, I. H.; Lee, H. Y.; Lee, H. D.; Jung, Y. J.; Tendler, S. J. B.; Williams, P. M.; Allen, S.; Ryu, S. H.; Park, J. W. Interactions between Signal-Transducing Proteins Measured by Atomic Force Microscopy. *Anal. Chem.* **2009**, *81*, 3276–3284.
47. Jung, Y. J.; Park, Y. S.; Yoon, K. J.; Kong, Y. Y.; Park, J. W.; Nam, H. G. Molecule-Level Imaging of Pax6 mRNA Distribution in Mouse Embryonic Neocortex by Molecular Interaction Force Microscopy. *Nucleic Acids Res.* **2009**, *37*, e10.
48. Kim, J. S.; Jung, Y. J.; Park, J. W.; Shaller, A. D.; Wan, W.; Li, A. D. Q. Mechanically Stretching Folded Nano-π-Stacks Reveals Pico-Newton Attractive Forces. *Adv. Mater.* **2009**, *21*, 786–789.
49. Florin, E. L.; Moy, V. T.; Gaub, H. E. Adhesion Forces between Individual Ligand-Receptor Pairs. *Science* **1994**, *264*, 415–417.
50. Lo, Y. S.; Huefner, N. D.; Chan, W. S.; Stevens, F.; Harris, J. M.; Beebe, T. P. Specific Interactions between Biotin and Avidin Studied by Atomic Force Microscopy Using the Poisson Statistical Analysis Method. *Langmuir* **1999**, *15*, 1373–1382.
51. Nikitenko, S. I.; Koltypin, Y.; Felner, I.; Yeshurun, I.; Shames, A. I.; Jiang, J. Z.; Markovich, V.; Gorodetsky, G.; Gedanken, A. Tailoring the Fe-Fe_3C Nanocrystalline Particles Prepared by Sonochemistry. *J. Phys. Chem. B* **2004**, *108*, 7620–7626.
52. Tsang, S. C.; Qiu, J.; Harris, P. J. F.; Fu, Q. J.; Zhang, N. Synthesis of Fullerenic Nanocapsules from Bio-Molecule Carbonization. *Chem. Phys. Lett.* **2000**, *322*, 553–560.
53. The magnetic moment of 12.1 nm MNP was estimated by considering the volume ratio between 10 nm MNP (2.5×10^{-19} A m^2) in the literature and the above.
54. The process of acquiring a tapping mode topographic image in air might induce damage to the molecular architecture at the tip end due to strong forces applied between the tip and substrate during tapping mode imaging. For this reason, specific DNA interaction forces were always recorded first in aqueous conditions, prior to recording MFM images in air.